Fluid Phase Equilibria 586 (2024) 114196

Contents lists available at ScienceDirect

Fluid Phase Equilibria

journal homepage: www.sciencedirect.com/journal/fluid-phase-equilibria

Extrapolating into no man's land enables accurate estimation of surface properties with multiparameter equations of state

Morten Hammer [a,b,*], Ailo Aasen [b], Øivind Wilhelmsen [a,b]

[a] Porelab, Department of Chemistry, Norwegian University of Science and Technology, NO 7491, Trondheim, Norway
[b] Department of Gas Technology, SINTEF Energy Research, NO 7465, Trondheim, Norway

ARTICLE INFO

Keywords:
Metastable
Surface tension
Equation of state
Multiparameter
Extrapolation
Unstable

ABSTRACT

Thermodynamic properties of homogeneous fluids in the metastable and unstable regions are needed to describe confined fluids, interfaces, nucleating embryos and estimate critical mass flow rates. The most accurate equations of state (EoS) called multiparameter EoS, have a second, non-physical Maxwell loop that renders predictions unreliable in these regions. We elaborate how information from the stable region can be used to reconstruct the metastable and unstable regions. For a simple interaction potential, comparison to results from molecular simulations reveals that isochoric expansion of the pressure from stable states reproduces simulation results in the metastable regions. By constructing a dome that extends above the critical point, we obtain an extrapolated pressure from multiparameter EoS that is free of second Maxwell loops. A reconstructed EoS is developed next, by integrating the extrapolated pressure from a stable state to obtain the Helmholtz energy. The consistency of the reconstructed EoS is gauged by computing phase equilibrium densities, pressures, and enthalpies of evaporation, which are in reasonable agreement with experimental values. Combined with density gradient theory, the reconstructed EoS yields surface tensions of water, carbon dioxide, ammonia, hydrogen and propane that deviate, on average, 4.4%, 1.6%, 6.0%, 0.7% and 5.4% from experimental values respectively. The results reveal a potential to develop more accurate extrapolation protocols, which can be leveraged to obtain prediction of metastable properties, surface properties or used as constraints in fitting multiparameter EoS.

1. Introduction

At isothermal conditions, homogeneous fluids with densities between the gas and liquid coexistence densities are either thermodynamically metastable or unstable with respect to separation into two phases [1–3]. The isotherm of CO_2 at 278.5 K is shown in Fig. 1. To the left and right of the two metastable regions (shaded light gray), the homogeneous fluid is thermodynamically stable and its properties can be characterized experimentally [4]. In the metastable regions, the nucleation barrier that must be overcome to form a second-phase may be large enough to allow sufficient time for experimental investigation [2,5–8]. However, the available time becomes exponentially smaller at higher metastablities [2,9], which constrains the region that can be examined experimentally. Due to the much shorter times needed in molecular simulations, thermodynamic properties at higher metastabilities can be studied [10–13].

Thermodynamic properties of metastable fluids are needed to overcome a myriad of scientific and industrial challenges [2,14–17]. In nucleation theory, the rate of formation of droplets depends on the pressure difference between the bulk liquid (stable) and the supersaturated gas (metastable) at the same intensive properties [17–19]. This is the case for formation of droplets in a supersaturated, metastable vapor-phase (to the left in Fig. 1), or formation of bubbles in a stretched, metastable liquid-phase (to the right in Fig. 1). In confined systems such as porous media, metastable fluids can be superstabilized by finite-size effects that suppress nucleation [20–22]. In flow through nozzles, the metastable properties of the fluid are needed to accurately characterize the critical mass flow rate [14,15,23]. Other examples where properties of metastable fluids are central is in melting point depletion in molecular clusters [24], capillary condensation and evaporation in nanoporous materials [25,26], delay of crystallization in small confinements [27,28] and vaporization around nanoparticles [29].

Thermodynamic properties of fluids in the unstable region are experimentally unavailable, and indeed not even well-defined. To make them well-defined requires restricting the allowable fluctuations, and molecular simulations techniques have been developed for this purpose [33,34]. The properties of fluids in the unstable region are used

* Corresponding author at: Porelab, Department of Chemistry, Norwegian University of Science and Technology, NO 7491, Trondheim, Norway.
E-mail address: morten.hammer@ntnu.no (M. Hammer).

https://doi.org/10.1016/j.fluid.2024.114196
Received 27 March 2024; Received in revised form 18 June 2024; Accepted 27 July 2024
Available online 30 July 2024

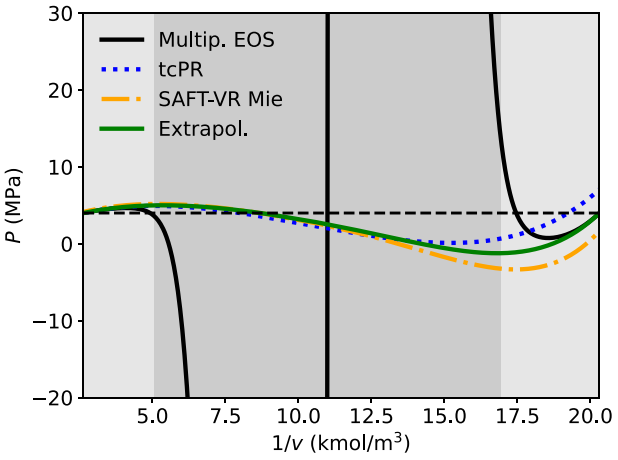

Fig. 1. Pressure as function of density for CO_2 at 278.5 K, from the multiparameter EoS by Span and Wagner [30] (black solid line), a first order extrapolation of the pressure (green solid line), SAFT-VR-Mie [31] (yellow dash-dot line) and translated–consistent Peng–Robinson [32] (tcPR) (blue dotted line), where the horizontal dashed line is the saturation pressure. The thermodynamically metastable and unstable regions are shaded light and dark gray respectively.

as input in at least two theoretical frameworks. Firstly, thermodynamic states in the unstable region are found across the vapor–liquid interface, where they are stabilized by the large density gradient. Their properties are used as input in theories to calculate interfacial properties such as density gradient theory (DGT) and density functional theory (DFT) for fluids. Another important application is description of mixtures. For equations of state (EoS) where the thermodynamic description of the mixture is developed on the basis of pure-component descriptions [4], the density of the mixture can be such that the pure-component description is evaluated in the unstable region [4].

The shape of the pressure as a function of density displayed by the curves from SAFT-VR Mie and translated–consistent Peng–Robinson (tcPR) [32] in Fig. 1 has a local maximum followed by a local minimum. This is called a "Maxwell loop". While these EoS have only one Maxwell loop, the multiparameter EoS for CO_2 [30] has two. Moreover, the second Maxwell loop diverges to very large values. This is not particular for CO_2, but a general characteristic of this type of EoS for most fluids, with a notable exception for some Mie fluids [35]. The second Maxwell loop seems to be an artifact of the functional form and parameterization [36]. Multiparameter EoS have unparalleled accuracy in the stable regions of the phase diagram. However, the second Maxwell loop renders their predictions unreliable in the metastable regions, prevents combination with DGT [36] to calculate surface properties, and causes problems in the description of mixtures [4,36].

In this work, we present a methodology that takes advantage of the high accuracy of multiparameter EoS in the stable region to reconstruct the thermodynamic properties in the metastable and unstable regions, referred to as the reconstructed EoS. We show that the reconstructed EoS reproduces phase equilibrium densities, pressures, and enthalpies of evaporation from experiments to a reasonable accuracy. Moreover, it is free of the second, non-physical Maxwell loop. This allows combination with DGT, which results in accurate representation of the surface tensions of several important fluids. The presented methodology opens the possibility to use multiparameter EoS for surface tension predictions, and to develop constraints in the metastable and unstable regions of the phase diagram that can be used in the regression of multiparameter EoS.

2. Theory

The methodology used in this work is conceptually outlined in Fig. 2. The first building block is an accurate extrapolation of the

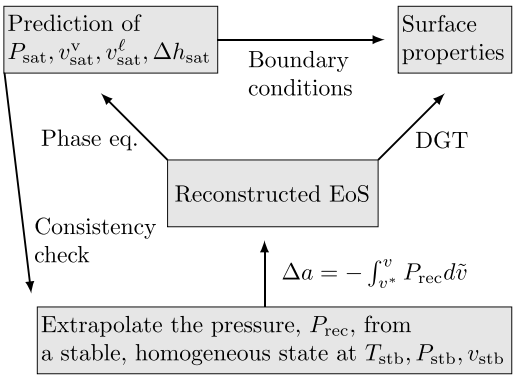

Fig. 2. The methodology for developing a reconstructed EoS and calculating surface properties.

pressure (or some other thermodynamic property) into the metastable and unstable regions from a stable, homogeneous state (superscript stb) at temperature, $T_{\rm stb}$, pressure, $P_{\rm stb}$ and molar volume, $v_{\rm stb}$. This will be discussed in Section 2.1. Three different choices of stable states will be discussed in Section 2.2. The next building block is the reconstructed EoS, which will be defined in Section 2.3. Eventually, the reconstructed EoS can be combined with phase-equilibrium calculations and DGT to calculate surface properties, as elaborated in Section 2.4.

2.1. The extrapolation

There are several ways to extrapolate into the metastable and unstable regions. Such extrapolations are discussed in detail for pure components and mixtures in Ref. [37], which is referred to for a more in-depth discussion. Comparison to results from molecular dynamics simulations for a simple fluid reveals that isochoric extrapolation of the pressure works well (see Ref. [37] and Section 3). To avoid extrapolating too far in temperature, the isochoric extrapolation should be performed from the closest possible temperature corresponding to a stable state. The pressure is then

$$P_{\rm rec}(T,v) = P_{\rm stb}(T_{\rm stb},v) + P_{{\rm stb},T}(T_{\rm stb},v)(T-T_{\rm stb}) + \frac{1}{2}P_{{\rm stb},TT}(T_{\rm stb},v)(T-T_{\rm stb})^2 \quad (1)$$

where subscript rec refers to the reconstructed EoS, and P_T and P_{TT} are the first and second order derivatives of the pressure with respect to the temperature, holding v constant. Including the two first terms on the right-hand-side results in a first-order extrapolation, and including all terms gives a second-order extrapolation. Eq. (1) represents one way to extrapolate into the metastable and unstable regions of the phase diagram that works well, but there are likely more sophisticated and accurate ways to accomplish the extrapolation, which is a promising topic for future research.

2.2. The choice of stable state

It is possible to characterize the thermodynamic properties very accurately in the stable regions, and multiparameter EoS usually accomplish this very well [4]. Close to the critical point, density fluctuations become very large and cause thermodynamic properties to approach the critical point with a non-analytic behavior. Multiparameter EoS can represent thermodynamic properties accurately also close to the critical point [4]. However, the non-analytic behavior in combination with possible inaccuracies in the EoS means that the extrapolation in Eq. (1) may be questionable if the stable state is too close to the critical point. To address this challenge, we shall examine three different choices of stable states:

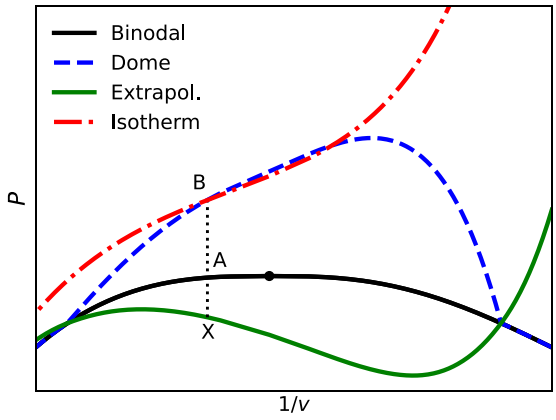

(a)

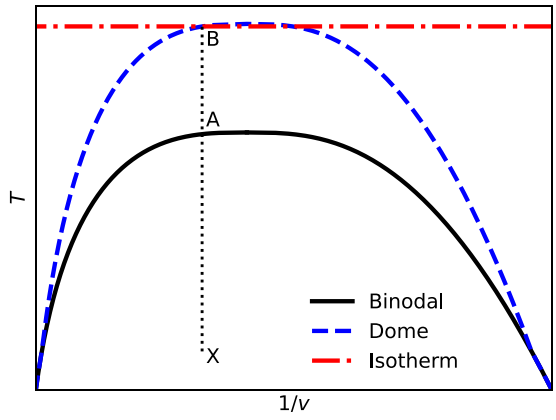

(b)

Fig. 3. Illustration of extrapolation from different states to State X: From the coexistence curve, State A (solid line), from a dome, State B (dashed line), and from a supercritical isotherm, State B (dash-dot line). In the illustration, State B is taken to be at the intersection of the dome and the supercritical isotherm. At different isochores than the one depicted in the illustration, State B from the dome and supercritical isotherm will differ.

Coexistence curve: $T_{\text{stb}}(v) = T_{\text{sat}}(v)$, where subscript sat refers to a state at the coexistence curve. An example is shown as State A in Fig. 3.

Dome: $T_{\text{stb}}(v) = T_{\text{sat}}(v) + \Delta T(v)$, where $\Delta T(v) = \max\left(0, \frac{(T_{\text{sat}}(v)-T_{\text{rec}})(T_{\text{max}}-T_{\text{c}})}{T_{\text{c}}-T_{\text{rec}}}\right)$ where T_c is the critical temperature. An example is shown as State B in Fig. 3. In this work we use $T_{\text{max}} = 1.1T_{\text{c}}$. More details motivating the choice of T_{max} can be found in the Supporting Information (SI).

Supercritical: $T_{\text{stb}}(v) = T_{\text{SC}}$, where T_{SC} is a constant temperature at supercritical conditions. An example is shown as State B in Fig. 3.

We see that the coexistence curve is closest to the state of interest (X), followed by the dome, with the supercritical isotherm having the largest distance. We shall use this to evaluate the sensitivity of the methodology with respect to the choice of stable states in Section 3.

2.3. The reconstructed EoS

With the pressure as a function of volume at a given temperature, T^*, the molar Helmholtz energy of the reconstructed EoS is

$$a_{\text{rec}}(T^*, v) = a^*(T^*, v^*) - \int_{v^*}^{v} P_{\text{rec}} d\tilde{v} \tag{2}$$

where subscript $*$ denotes the reference state, which is taken to be the molar Helmholtz energy of the EoS at the stable state (T^*, v^*). This gives the following chemical potential

$$\mu_{\text{rec}}(T^*, v) = \mu^*(T^*, v^*) + \int_{v^*}^{v} \tilde{v} P_{\text{rec},\tilde{v}}\, d\tilde{v} \tag{3}$$

where subscript $\tilde{v}$ refers to the derivative with respect to the molar volume. The molar entropy is

$$s_{\text{rec}}(T^*, v) = s^*(T^*, v^*) + \int_{v^*}^{v} P_{\text{rec},T}\, d\tilde{v}. \tag{4}$$

Other thermodynamic properties can readily be calculated as

$$u_{\text{rec}}(T^*, v) = a_{\text{rec}} + T^* s_{\text{rec}} \tag{5}$$

$$h_{\text{rec}}(T^*, v) = \mu_{\text{rec}} + T^* s_{\text{rec}} \tag{6}$$

$$g_{\text{rec}}(T^*, v) = \mu_{\text{rec}} \tag{7}$$

where u, h, g are the molar internal energy, enthalpy and Gibbs energy. We let the reference state be the stable state of the gas-phase, defined in Section 2.2.

2.4. Phase equilibrium and surface properties with DGT

The reconstructed EoS is not identical to the original EoS. While the thermodynamic properties at the reference state in the gas phase with superscript $*$ is identical to the original EoS, the chemical potential of the liquid-phase from the reconstructed EoS results from an integration across the metastable and unstable regions. The phase equilibrium conditions for the reconstructed EoS are

$$\mu_{\text{rec}}(v^{\text{v}}) = \mu_{\text{rec}}(v^{\ell}), \tag{8}$$

$$P_{\text{rec}}(v^{\text{v}}) = P_{\text{rec}}(v^{\ell}). \tag{9}$$

where superscripts v and ℓ refer to the gas and liquid phases respectively. Comparison of the solutions from Eqs. (8)–(9) and the equivalent quantities from the original EoS with those obtained from the reconstructed EoS can be used to gauge the precision of the extrapolation from Section 2.1.

Also the enthalpy of evaporation from the reconstructed EoS results from an integration across the metastable and unstable regions of the phase diagram (see Eqs. (4) and (6)). Hence, to compare the predictions from the reconstructed EoS to values form the original EoS serves as another consistency check of the extrapolation from Section 2.1.

3. Results and discussion

We start by gauging the accuracy of the extrapolation in Eq. (1) by comparing to results from molecular simulations in the metastable regions (Section 3.1). We evaluate next how the choice of stable state influences the predictions of thermodynamic properties by the reconstructed EoS (Section 3.2). Eventually, we assess the ability of the reconstructed EoS combined with DGT to represent surface properties (Section 3.3). All calculations in this work have been performed using the thermodynamic software Thermopack [36,38].

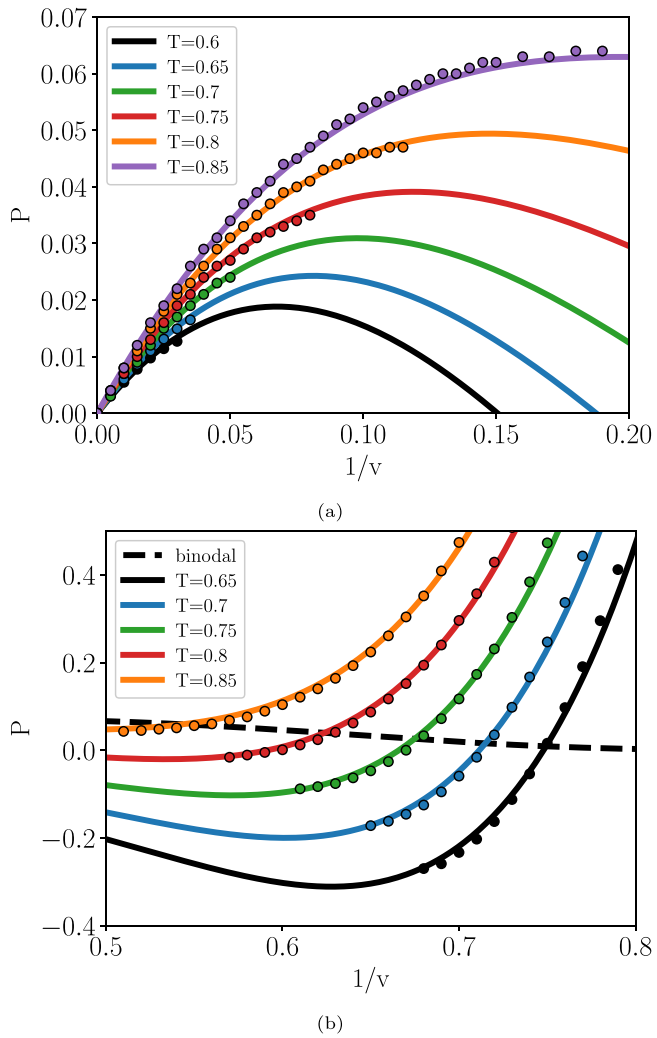

Fig. 4. Comparison of an extrapolation from the binodal with Eq. (1) for the Lennard-Jones spline fluid at different temperatures with molecular simulation results from Ref. [12]. The dashed line represents the coexistence pressure.

3.1. Isochoric extrapolation of the pressure

Since thermodynamic properties of metastable fluids are scarce, we will rely on results from molecular simulations to demonstrate the suitability of the extrapolation discussed in Section 2.1. For a more in-depth discussion of the extrapolation in Eq. (1) for pure components and mixtures, we refer to Ref. [37]. There are experimental data available for real fluids, also for thermodynamic properties in the metastable regions [2], but only at relatively low metastabilities [39]. Molecular simulations offer the possibility to study homogeneous fluids at higher metastabilities.

The Lennard Jones spline (LJ/s) potential is a Lennard Jones potential truncated in a unique way, which makes the interaction potential and the force continuous [40]. As such, it avoids the need for further specification and risk of ambiguity in how the potential is used in a simulation. In 2022, van Westen and collaborators presented an accurate EoS based on thermodynamic perturbation theory for the Lennard-Jones spline (LJ/s) fluid [12]. Using the accurate perturbation theory by van Westen et al. to calculate thermodynamic properties in the stable region at the coexistence curve [12], we estimate the pressure in the metastable and unstable regions of the phase diagram as explained in Section 2. Fig. 4 reveals a remarkable correspondence between the extrapolation and molecular simulation results from Ref. [12] in the metastable regions of the gas-phase (Fig. 4(a)) and the liquid-phase (Fig. 4(b)). Moreover, the extrapolation has a single Maxwell loop, unlike the multiparameter EoS for CO_2 shown in Fig. 1. These results support the use of the extrapolation in reconstructing thermodynamic properties in the metastable and unstable regions. We proceed to discuss the use of the extrapolation to develop reconstructed EoS for real fluids.

3.2. Evaluating the choice of stable state

Fig. 1 compares isochoric extrapolation of the pressure to the corresponding pressures from the multiparameter EoS for CO_2 at T = 278.5 K. While the multiparameter EoS has two Maxwell loops with pressures that diverge to very large absolute values, the isochoric extrapolation based on *exactly the same* EoS in the stable region, has a physically admissible behavior with a single Maxwell loop that appears to be well-behaved.

While this is true for many fluids and conditions, we find that using stable states in vicinity of the critical point from multiparameter EoS, can result in non-physical behavior for the extrapolated pressure. An example of this is shown in the SI. We hypothesize that this is either due to inaccuracies in the EoS, or due to critical behavior in this region that renders the stable states in vicinity of the critical point unsuitable as starting points for the extrapolation. For instance, close to the critical point, density fluctuations become very large and cause thermodynamic properties to approach the critical point with a non-analytic behavior.

Hence, using the phase envelope as starting point for the extrapolation when combined with multiparameter EoS can yield artifacts in the extrapolated pressure in the unstable region (the dark gray region in Fig. 1). This is avoided by using either the dome presented in Section 2.2, or a supercritical isotherm at sufficiently high temperature to define the stable states. We emphasize that extrapolating from the phase envelope is clearly preferred to calculate thermodynamic properties of metastable states, and this works very well, as shown in Fig. 4. However, we proceed to investigate a dome and a supercritical isotherm to describe also the unstable region and to allow calculation of surface properties in Section 3.3.

We combine the extrapolation in Eq. (1) with the multiparameter EoS for hydrogen [41], carbon dioxide [30], water [42], ammonia [43] and propane [44], and use the procedure outlined in Section 2.3 to develop reconstructed EoS for these fluids. Eqs. (8) and (9) provide an opportunity to evaluate the reliability of the reconstructed EoS.

The phase equilibrium conditions and the enthalpy of evaporation from the reconstructed EoS should agree with results from the multiparameter EoS. Since the reconstructed EoS obtains the chemical potential and enthalpy differences between the gas and liquid by integrating through the metastable and unstable domains of the homogeneous fluid (see Eq. (3)), this consistency check is quite stringent.

A comparison is shown in Fig. 5. The enthalpy of evaporation in Fig. 5(c) shows that the accuracy of the reconstructed EoS is influenced by the choice of stable state. The dome is a better choice than the supercritical isotherm, which is expected as it lies closer to the end states, as illustrated in Fig. 3. Fig. 5 suggests that there is a reasonable agreement between the reconstructed EoS and the multiparameter EoS. The Mean Average Percentage Deviation (MAPD) of the reconstructed EoS is shown in Table 1. Using domes to define the stable states, the enthalpy of evaporation is reproduced within a good accuracy, with MAPD's varying from 1.9% for CO_2 and propane, to 6.5% for water. The saturation volume of the liquid-phase is represented within 0.1%. Larger deviations are seen for the saturation pressures and gas-phase volumes, where the gas-phase saturation volume of water has an MAPD as large as 23%, while the MAPD of CO_2 is only 1.8%. This is in-line with the discussion in Ref. [37], which specifically points out a potential for improvement of the extrapolation protocol for metastable vapor.

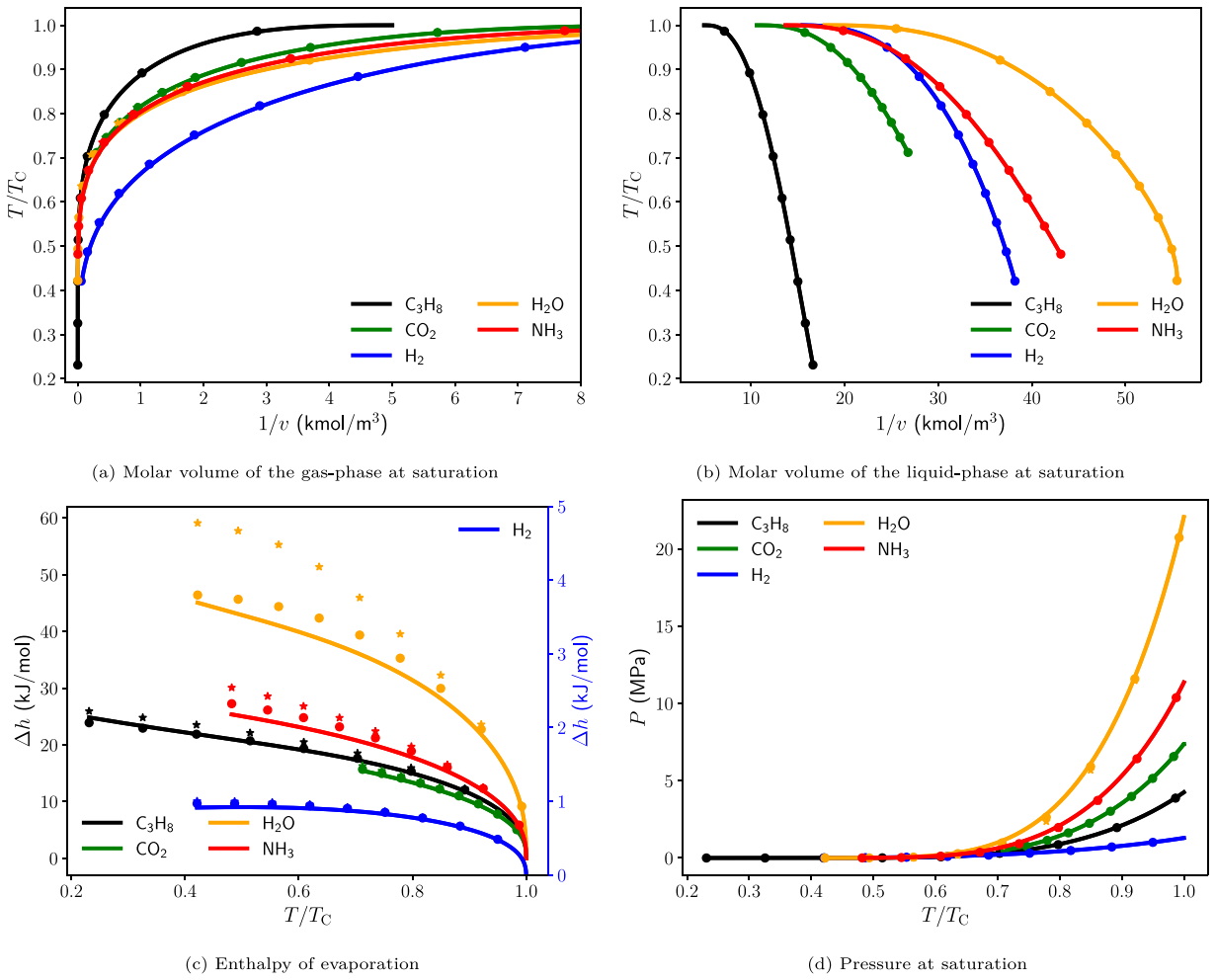

(a) Molar volume of the gas-phase at saturation

(b) Molar volume of the liquid-phase at saturation

(c) Enthalpy of evaporation

(d) Pressure at saturation

Fig. 5. Prediction of saturation properties with the reconstructed EoS for water, carbon dioxide, ammonia, hydrogen and propane with stable states from a supercritical isotherm (filled stars) or from a dome (filled circles), compared with results from the multiparameter EoS (solid lines). In (c), the enthalpy of evaporation of hydrogen has a separate axis due to its small value.

Table 1
Mean absolute percentage deviation for selected thermodynamic properties at saturation with the reconstructed EoS.

Property (Case)	H_2O	CO_2	NH_3	H_2	C_3H_8
P_{sat} (Dome)	15.7	1.28	11.2	4.64	5.94
P_{sat} (Supercritical)	43.8	2.96	20.6	6.82	26.8
v^v_{sat} (Dome)	23.2	1.83	15.5	5.63	5.88
v^v_{sat} (Supercritical)	99.7	4.00	39.8	8.68	70.8
v^ℓ_{sat} (Dome)	0.0975	0.0458	0.0632	0.0231	0.0551
v^ℓ_{sat} (Supercritical)	0.0475	0.0332	0.0274	0.0261	0.0662
Δh_{sat} (Dome)	6.56	1.94	6.08	3.49	1.91
Δh_{sat} (Supercritical)	23.3	3.94	11.9	5.02	6.16

Stronger attraction between the molecules generally leads to larger enthalpies of evaporation and a higher saturation pressure at the same reduced temperature. This trend is also apparent in Fig. 5, where the hydrogen bonds of the water and ammonia molecules lead to strong interactions, while the hydrogen molecules have the weakest interactions. Fig. 5 and Table 1 suggest that the reconstructed EoS is most accurate for fluids with weaker interactions.

Table 2 and Fig. 5 shows that although the performance of the reconstructed EoS appears to be reliable, there is a potential for improvement of the extrapolation protocol, in particular for the gas phase. Future work could explore new extrapolation protocols, and use the methodology outlined in Fig. 2 and demonstrated in this work to gauge the accuracy and reliability of the reconstructed EoS.

3.3. Surface properties from DGT

Since the reconstructed EoS derived on the basis of the multiparameter EoS has a single Maxwell loop, it can be combined with density gradient theory (DGT) to estimate interfacial properties such as the surface tension. To evaluate this ability, the surface tensions calculated using the methodology described in Section 2.4 have been compared to the correlations by Mulero et al. [45] at 9 equidistant temperatures. The lowest temperature is the triple point temperature, and the other temperatures are calculated using $\Delta T = (T_c - T_{tr})/9$. The influence parameter, κ, in DGT has been fitted to reproduce the surface tension values from the correlations by Mulero et al. [45] at the second lowest temperature for all fluids. The influence parameters used with the reconstructed EoS are tabulated in the Supporting Information (SI). Together with the mean absolute percentage deviations (MAPD) reported in Table 2, we have also included for comparison predictions from the translated–consistent Peng–Robinson (tcPR) [32] EoS fitted by using the same methodology.

It is clear from Fig. 6 and the MAPD reported in Table 2 that the reconstructed EoS predicts surface tensions with a good accuracy, which significantly outperforms DGT combined with tcPR. Most notable are the improvements for CO_2 and H_2, where predictions from DGT using the reconstructed EoS are within the experimental accuracy (Compare the MAPD's from Table 2 with those reported in Tab. 2 of Ref. [45]).

Even though isochoric expansion works well, it is not perfect. There is a potential to further improve the accuracy of the methodology used

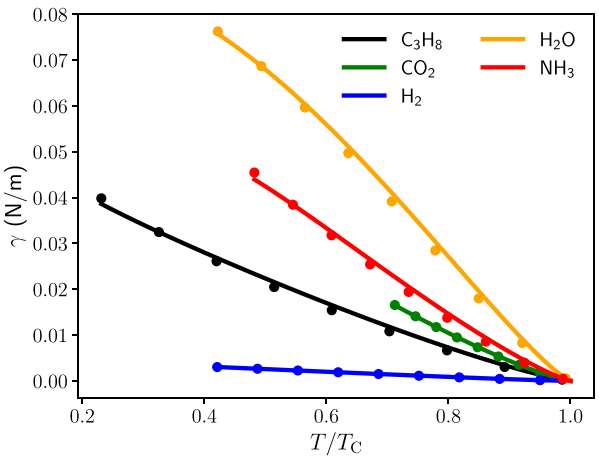

Fig. 6. Surface tension predictions for water, carbon dioxide, ammonia, hydrogen and propane. The solid lines plot the correlations from Mulero et al. [45] and the dots result from combining the extrapolated EoS with DGT. A new correlation was made for propane using data from Ref. [50], since the original correlation did not cover temperatures below 193.15 K. The new correlation is described in the SI.

Table 2
Mean absolute percentage deviation for the surface tension predictions with respect to the correlations from Mulero et al. [45], resulting from combining the reconstructed EoS or tcPR with DGT and using a constant influence parameter. The values of the influence parameters are provided in the Supporting Information.

Fluid	H_2O	CO_2	NH_3	H_2	C_3H_8
Reconstructed EoS	4.44	1.59	6.04	0.744	5.44
tcPR	23.2	9.78	15.2	7.29	11.1

to extrapolate into the metastable and unstable regions from the stable thermodynamic region by taking advantage of constraints offered by statistical mechanics, physical considerations and thermodynamics. A more accurate extrapolation will increase the accuracy of the reconstructed EoS, and enable the calculation of more accurate interfacial properties. This may allow other surface properties like adsorptions, Tolman lengths [46] and rigidity constants [47,48] to be estimated with higher accuracy, also for mixtures [49]. This could be leveraged to e.g. improve nucleation theory [9].

4. Conclusions

Thermodynamic properties of fluids in the metastable and unstable regions of the phase diagram of homogeneous fluids are needed in a wide range of applications. It has been shown that isochoric extrapolation of the pressure reproduces the pressure in the metastable region obtained from molecular dynamics simulations using the Lennard-Jones spline potential.

In this work, we have presented a methodology to develop a reconstructed equation of state (EoS) that combines a second order temperature expansion of the pressure with an accurate representation in the stable region to calculate thermodynamic properties in the metastable and unstable regions of the phase diagram of the homogeneous fluid.

Unlike the most accurate equations of state (EoS) available, namely multiparameter EoS, the reconstructed EoS has a physical admissible behavior with a single Maxwell loop. To achieve this, the stable states in the extrapolation of the pressure had to be taken from a dome that extended above the critical point.

We gauged the accuracy and consistency of the reconstructed EoS by self-consistently computing phase equilibrium volumes, pressures, and enthalpies of evaporation. The mean average percentage deviation (MAPD) of the saturation pressure, gas-phase volumes, liquid-phase volumes and enthalpies of evaporation varied between 1.3–15.7%, 1.8%–23%, 0.02–0.1% and 1.9–6.6% respectively, depending on the fluid. It was shown that this accuracy depended on the choice for defining the stable states. The reconstructed EoS appeared to be best for fluids with weaker attractive forces between the molecules like hydrogen and CO_2, with the largest deviations for water and ammonia that have hydrogen bonds.

The reconstructed EoS was eventually combined with density gradient theory to calculate surface tensions. This yielded surface tensions of H_2O, CO_2, NH_3, hydrogen and propane that deviate, on average, 4.4%, 1.6%, 6.0%, 0.7% and 5.4% from experimentally validated correlations respectively. This was significantly better than calculations performed by combining the translated–consistent Peng–Robinson equation of state with density gradient theory.

The results revealed a potential to develop more accurate extrapolation protocols, which could be exploited to achieve a higher accuracy for the reconstructed EoS. This can in the future be leveraged to obtain more precise prediction of metastable properties, surface properties or used as constraints in fitting multiparmeter EoS.

CRediT authorship contribution statement

Morten Hammer: Writing – review & editing, Writing – original draft, Visualization, Software, Methodology, Investigation, Conceptualization. **Ailo Aasen:** Writing – review & editing, Visualization, Methodology, Investigation, Conceptualization. **Øivind Wilhelmsen:** Writing – review & editing, Writing – original draft, Visualization, Methodology, Investigation, Conceptualization.

Declaration of competing interest

The authors declare the following financial interests/personal relationships which may be considered as potential competing interests: Morten Hammer reports financial support was provided by European Research Council. Morten Hammer reports financial support was provided by Research Council of Norway. Ailo Aasen reports financial support was provided by Research Council of Norway. Oivind Wilhelmsen reports financial support was provided by European Research Council. Oivind Wilhelmsen reports financial support was provided by Research Council of Norway. If there are other authors, they declare that they have no known competing financial interests or personal relationships that could have appeared to influence the work reported in this paper.

Data availability

Data will be made available on request.

Acknowledgments

This work has received funding from the European Research Council (ERC) under the European Union's Horizon Europe research and innovation program (grant agreement No. 101115669) and from the European Union's Horizon 2020 research and innovation programme under grant agreement no. 101022487 (ACCSESS project). The work was partly supported by the Research Council of Norway through its Centres of Excellence funding scheme, Porelab, Project Number 262644, and the project Monitoring and control networks for CCS (MACON CCS), Project Number 327056.

Appendix A. Supplementary data

Supplementary material related to this article can be found online at https://doi.org/10.1016/j.fluid.2024.114196.

References

[1] H.B. Callen, Thermodynamics and an Introduction to Thermostatistics, John Wiley & Sons, New York, 1985.

[2] P.G. Debenedetti, Metastable Liquids: Concepts and Principles, Princeton University Press, Princeton, 1996.

[3] P. Aursand, M. Aa. Gjennestad, E. Aursand, M. Hammer, Ø. Wilhelmsen, The spinodal of single- and multi-component fluids and its role in the development of modern equations of state, Fluid Phase Equilib. 436 (2017) 98–112, http://dx.doi.org/10.1016/j.fluid.2016.12.018.

[4] R. Span, Multiparameter Equations of State, Springer-Verlag, Berlin, 2000, http://dx.doi.org/10.1007/978-3-662-04092-8.

[5] V. Bayudakov, V. Skripov, Superheating and surface tension of vapor nuclei of nitrogen, oxygen, and methane, Zh. Fiz. Khim. (1982).

[6] V.G. Baidakov, V.E. Vinogradov, P.A. Pavlov, Limiting tensile strength of liquid nitrogen, Phys. Fluids 28 (5) (2016) http://dx.doi.org/10.1063/1.4951703.

[7] V. Baidakov, A. Pankov, Attainable superheat of ethane-methane solutions, Thermophys. Aeromechanics 20 (2013) 399–406, http://dx.doi.org/10.1134/S0869864313040021.

[8] V. Baidakov, A. Kaverin, A. Pankov, Spontaneous boiling-up of gas-saturated liquids: Attainable superheating of ethane–helium and ethane–hydrogen solutions, Int. J. Heat Mass Transfer 221 (2024) 125050, http://dx.doi.org/10.1016/j.ijheatmasstransfer.2023.125050.

[9] A. Aasen, D. Reguera, Ø. Wilhelmsen, Curvature corrections remove the inconsistencies of binary classical nucleation theory, Phys. Rev. Lett. 124 (2020) 045701, http://dx.doi.org/10.1103/PhysRevLett.124.045701.

[10] P.H. Poole, F. Sciortino, U. Essmann, H.E. Stanley, Phase behaviour of metastable water, Nature 360 (6402) (1992) 324–328, http://dx.doi.org/10.1038/360324a0.

[11] A. Keller, K. Langenbach, H. Hasse, Comparison of predictions of the PC-SAFT equation of state and molecular simulations for the metastable region of binary mixtures, Fluid Phase Equilib. 444 (2017) 31–36, http://dx.doi.org/10.1016/j.fluid.2017.04.009.

[12] T. Van Westen, M. Hammer, B. Hafskjold, A. Aasen, J. Gross, Ø. Wilhelmsen, Perturbation theories for fluids with short-ranged attractive forces: A case study of the Lennard-Jones spline fluid, J. Chem. Phys. 156 (10) (2022) http://dx.doi.org/10.1063/5.0082690.

[13] J. Puibasset, P. Judeinstein, J.-M. Zanotti, Molecular simulation study of the heat capacity of metastable water between 100 and 300 k, Mol. Simul. 45 (4–5) (2019) 462–465, http://dx.doi.org/10.1080/08927022.2018.1535179.

[14] Ø. Wilhelmsen, A. Aasen, K. Banasiak, H. Herlyng, A. Hafner, One-dimensional mathematical modeling of two-phase ejectors: Extension to mixtures and mapping of the local exergy destruction, Appl. Therm. Eng. 217 (2022) 119228, http://dx.doi.org/10.1016/j.applthermaleng.2022.119228.

[15] Ø. Wilhelmsen, A. Aasen, Choked liquid flow in nozzles: Crossover from heterogeneous to homogeneous cavitation and insensitivity to depressurization rate, Chem. Eng. Sci. 248 (2022) 117176, http://dx.doi.org/10.1016/j.ces.2021.117176.

[16] S. Balibar, F. Caupin, Metastable liquids, J. Phys.: Condens. Matter. 15 (1) (2002) S75, http://dx.doi.org/10.1088/0953-8984/15/1/308.

[17] J. Wedekind, D. Reguera, R. Strey, Finite-size effects in simulations of nucleation, J. Chem. Phys. 125 (21) (2006) http://dx.doi.org/10.1063/1.2402167.

[18] A. Aasen, Ø. Wilhelmsen, M. Hammer, D. Reguera, Free energy of critical droplets—from the binodal to the spinodal, J. Chem. Phys. 158 (11) (2023) http://dx.doi.org/10.1063/5.0142533.

[19] H. Vehkamäki, I.J. Ford, Analysis of water–ethanol nucleation rate data with two component nucleation theorems, J. Chem. Phys. 113 (8) (2000) 3261–3269, http://dx.doi.org/10.1063/1.1286965.

[20] Ø. Wilhelmsen, D. Bedeaux, S. Kjelstrup, D. Reguera, Communication: Supersaturation of fluids in nanocontainer, J. Chem. Phys. 141 (2014) 071103, http://dx.doi.org/10.1063/1.4893701.

[21] F. Caupin, Effects of compressibility and wetting on the liquid–vapor transition in a confined fluid, J. Chem. Phys. 157 (5) (2022) http://dx.doi.org/10.1063/5.0098969.

[22] P. Montero de Hijes, C. Vega, On the thermodynamics of curved interfaces and the nucleation of hard spheres in a finite system, J. Chem. Phys. 156 (1) (2022) http://dx.doi.org/10.1063/5.0072175.

[23] M. Hammer, H. Deng, A. Austegard, A.M. Log, S.T. Munkejord, Experiments and modelling of choked flow of CO_2 in orifices and nozzles, Int. J. Multiph. Flow 156 (2022) 104201, http://dx.doi.org/10.1016/j.ijmultiphaseflow.2022.104201.

[24] M. Schmidt, R. Kusche, T. Hippler, J. Donges, W. Kronmüller, B. Von Issendorff, H. Haberland, Negative heat capacity for a cluster of 147 sodium atoms, Phys. Rev. Lett. 86 (7) (2001) 1191, http://dx.doi.org/10.1103/PhysRevLett.86.1191.

[25] T. Horikawa, D. Do, D. Nicholson, Capillary condensation of adsorbates in porous materials, Adv. Colloid Interface Sci. 169 (1) (2011) 40–58, http://dx.doi.org/10.1016/j.cis.2011.08.003.

[26] C.J. Rasmussen, A. Vishnyakov, M. Thommes, B.M. Smarsly, F. Kleitz, A.V. Neimark, Cavitation in metastable liquid nitrogen confined to nanoscale pores, Langmuir 26 (12) (2010) 10147–10157, http://dx.doi.org/10.1021/la100268q.

[27] M. Beiner, Rengarajan, S. Pankaj, D. Enke, M. Steinhart, Manipulating the crystalline state of pharmaceuticals by nanoconfinement, Nano Lett. 7 (5) (2007) 1381–1385, http://dx.doi.org/10.1021/nl0705081.

[28] R. Grossier, Z. Hammadi, R. Morin, S. Veesler, Predictive nucleation of crystals in small volumes and its consequences, Phys. Rev. Lett. 107 (2) (2011) 025504, http://dx.doi.org/10.1103/PhysRevLett.107.025504.

[29] M.T. Carlson, A.J. Green, H.H. Richardson, Superheating water by cw excitation of gold nanodots, Nano Lett. 12 (3) (2012) 1534–1537, http://dx.doi.org/10.1021/nl2043503.

[30] R. Span, W. Wagner, A new equation of state for carbon dioxide covering the fluid region from the triple-point temperature to 1100 k at pressures up to 800 MPa, J. Phys. Chem. Ref. Data 25 (1996) 1509, http://dx.doi.org/10.1063/1.555991.

[31] T. Lafitte, A. Apostolakou, C. Avendaño, A. Galindo, C.S. Adjiman, E.A. Müller, G. Jackson, Accurate statistical associating fluid theory for chain molecules formed from mie segments, J. Chem. Phys. 139 (15) (2013) 154504, http://dx.doi.org/10.1063/1.4819786.

[32] Y. Le Guennec, R. Privat, J.-N. Jaubert, Development of the translated-consistent tc-PR and tc-RK cubic equations of state for a safe and accurate prediction of volumetric, energetic and saturation properties of pure compounds in the sub-and super-critical domains, Fluid Phase Equilib. 429 (2016) 301–312, http://dx.doi.org/10.1016/j.fluid.2016.09.003.

[33] D.S. Corti, P.G. Debenedetti, A computational study of metastability in vapor—liquid equilibrium, Chem. Eng. Sci. 49 (17) (1994) 2717–2734, http://dx.doi.org/10.1016/0009-2509(94)E0093-6.

[34] J.P. Valleau, Temperature-and-density-scaling Monte Carlo: Methodology and the canonical thermodynamics of lennard-jonesium, Mol. Simul. 31 (4) (2005) 223–253, http://dx.doi.org/10.1080/08927020500035937.

[35] S. Pohl, R. Fingerhut, M. Thol, J. Vrabec, R. Span, Equation of state for the mie (λr, 6) fluid with a repulsive exponent from 11 to 13, J. Chem. Phys. 158 (8) (2023) http://dx.doi.org/10.1063/5.0133412.

[36] Ø. Wilhelmsen, A. Aasen, G. Skaugen, P. Aursand, A. Austegard, E. Aursand, M.A. Gjennestad, H. Lund, G. Linga, M. Hammer, Thermodynamic modeling with equations of state: Present challenges with established methods, Ind. Eng. Chem. Res. 56 (13) (2017) 3503–3515, http://dx.doi.org/10.1021/acs.iecr.7b00317.

[37] A. Aasen, D. Reguera, M. Hammer, W. Ø., Estimating metastable thermodynamic properties by isochoric extrapolation, J. Chem. Phys. 161 (4) (2024) 044113, http://dx.doi.org/10.1063/5.0220207.

[38] Thermopack open-source thermodynamics library, https://github.com/thermotools/thermopack/ (2020).

[39] R. Speedy, C. Angell, Isothermal compressibility of supercooled water and evidence for a thermodynamic singularity at 45 °c, J. Chem. Phys. 65 (3) (1976) 851–858, http://dx.doi.org/10.1063/1.433153.

[40] B. Hafskjold, K.P. Travis, A.B. Hass, M. Hammer, A. Aasen, Ø.ivind. Wilhelmsen, Thermodynamic properties of the 3D Lennard-Jones/spline model, Mol. Phys. 117 (23–24) (2019) 3754–3769, http://dx.doi.org/10.1080/00268976.2019.1664780.

[41] J.W. Leachman, R.T. Jacobsen, S.G. Penoncello, E.W. Lemmon, Fundamental equations of state for parahydrogen, normal hydrogen, and orthohydrogen, J. Phys. Chem. Ref. Data 38 (2009) 721, http://dx.doi.org/10.1063/1.3160306.

[42] W. Wagner, A. Pruß, The IAPWS formulation 1995 for the thermodynamic properties of ordinary water substance for general and scientific use, J. Phys. Chem. Ref. Data 31 (2002) 387, http://dx.doi.org/10.1063/1.1461829.

[43] K. Gao, J. Wu, I.H. Bell, A.H. Harvey, E.W. Lemmon, A reference equation of state with an associating term for the thermodynamic properties of ammonia, J. Phys. Chem. Ref. Data 52 (1) (2023) http://dx.doi.org/10.1063/5.0128269.

[44] E.W. Lemmon, M.O. McLinden, W. Wagner, Thermodynamic properties of propane. III. A reference equation of state for temperatures from the melting line to 650 k and pressures up to 1000 MPa, J. Chem. Eng. Data 54 (2009) 3141–3180, http://dx.doi.org/10.1021/je900217v.

[45] A. Mulero, I. Cachadiña, M. Parra, Recommended correlations for the surface tension of common fluids, J. Phys. Chem. Ref. Data 41 (4) (2012) 043105, http://dx.doi.org/10.1063/1.4768782.

[46] R.C. Tolman, The effect of droplet size on surface tension, J. Chem. Phys. 17 (3) (1949) 333–337, http://dx.doi.org/10.1063/1.1747247.

[47] E.M. Blokhuis, A.E. van Giessen, Density functional theory of a curved liquid-vapour interface: Evaluation of the rigidity constants, J. Phys.: Condens. Matter. 25 (2013) 225003, http://dx.doi.org/10.1088/0953-8984/25/22/225003.

[48] P. Rehner, A. Aasen, Ø. Wilhelmsen, Tolman lengths and rigidity constants from free-energy functionals–general expressions and comparison of theories, J. Chem. Phys. 151 (24) (2019) 244710, http://dx.doi.org/10.1063/1.5135288.

[49] A. Aasen, E.M. Blokhuis, Ø. Wilhelmsen, Tolman lengths and rigidity constants of multicomponent fluids: Fundamental theory and numerical examples, J. Chem. Phys. 148 (20) (2018) 204702, http://dx.doi.org/10.1063/1.5026747.

[50] V.N. Andbaeva, V.G. Baidakov, Capillary constant and surface tension of propane (R-290) with small additives of hydrogen, Fuel 287 (2021) 119546, http://dx.doi.org/10.1016/j.fuel.2020.119546.